AGU PUBLICATIONS

JGR

Journal of Geophysical Research: Biogeosciences

RESEARCH ARTICLE
10.1002/2015JG002943

Key Points:
- A new method was developed to estimate age-dependent forest C sink
- Quantitative relationship between forest age and C sink was revealed
- The dynamic of C sinks in vegetation and soil is significantly different

Supporting Information:
- Supporting Information S1

Correspondence to:
T. Zhou,
tzhou@bnu.edu.cn

Citation:
Zhou, T., P. Shi, G. Jia, Y. Dai, X. Zhao, W. Shangguan, L. Du, H. Wu, and Y. Luo (2015), Age-dependent forest carbon sink: Estimation via inverse modeling, *J. Geophys. Res. Biogeosci.*, *120*, doi:10.1002/2015JG002943.

Received 7 FEB 2015
Accepted 3 NOV 2015
Accepted article online 10 NOV 2015

Age-dependent forest carbon sink: Estimation via inverse modeling

Tao Zhou[1], Peijun Shi[1], Gensuo Jia[2], Yongjiu Dai[3], Xiang Zhao[4], Wei Shangguan[3], Ling Du[1], Hao Wu[1], and Yiqi Luo[5]

[1]State Key Laboratory of Earth Surface Processes and Resource Ecology, Beijing Normal University, Beijing, China, [2]TEA, Institute of Atmospheric Physics, Chinese Academy of Sciences, Beijing, China, [3]College of Global Change and Earth System Science, Beijing Normal University, Beijing, China, [4]State Key Laboratory of Remote Sensing Science, School of Geography, Beijing Normal University, Beijing, China, [5]Department of Microbiology and Plant Biology, University of Oklahoma, Norman, Oklahoma, USA

Abstract Forests have been recognized to sequester a substantial amount of carbon (C) from the atmosphere. However, considerable uncertainty remains regarding the magnitude and time course of the C sink. Revealing the intrinsic relationship between forest age and C sink is crucial for reducing uncertainties in prediction of forest C sink potential. In this study, we developed a stepwise data assimilation approach to combine a process-based Terrestrial ECOsystem Regional model, observations from multiple sources, and stochastic sampling to inversely estimate carbon cycle parameters including carbon sink at different forest ages for evergreen needle-leaved forests in China. The new approach is effective to estimate age-dependent parameter of maximal light-use efficiency ($R^2 = 0.99$) and, accordingly, can quantify a relationship between forest age and the vegetation and soil C sinks. The estimated ecosystem C sink increases rapidly with age, peaks at 0.451 kg C m^{-2} yr^{-1} at age 22 years (ranging from 0.421 to 0.465 kg C m^{-2} yr^{-1}), and gradually decreases thereafter. The dynamic patterns of C sinks in vegetation and soil are significantly different. C sink in vegetation first increases rapidly with age and then decreases. C sink in soil, however, increases continuously with age; it acts as a C source when the age is less than 20 years, after which it acts as a sink. For the evergreen needle-leaved forest, the highest C sink efficiency (i.e., C sink per unit net primary productivity) is approximately 60%, with age between 11 and 43 years. Overall, the inverse estimation of carbon cycle parameters can make reasonable estimates of age-dependent C sequestration in forests.

1. Introduction

The forest ecosystem plays a significant role in long-term carbon (C) sequestration [*Pan et al.*, 2011] and the mitigation of global warming caused by anthropogenically emitted carbon dioxide [*Intergovernmental Panel on Climate Change*, 2007]. However, considerable uncertainty remains regarding the fate of this forest C sink over both short and long timescales [*Luyssaert et al.*, 2007]. And the best way to manage forests to store C and to mitigate climate change is hotly debated [*Bellassen and Luyssaert*, 2014]. Because the net C accumulation by an ecosystem depends more heavily on forest age than on climate over long time scales [*Chapin et al.*, 2002], the improved understanding of forest age in influencing forest production, decomposition, and net C gain/loss is crucial for both quantification of long-term forest C sequestration and forest management under climate change [*Pregitzer and Euskirchen*, 2004; *Hui et al.*, 2012; *Anderson-Teixeira et al.*, 2013]. The quantitative relationship between the C sink (i.e., net ecosystem production (NEP)) and forest age is also important for parameterization of forest growth processes in carbon cycle models [*Ryan et al.*, 1997; *Williams et al.*, 2012] and for determination of relative influence of climate and disturbance on C stocks and fluxes [*Law et al.*, 2004].

The magnitude of a forest C sink is determined by a combination of intrinsic factors, which are commonly represented by the empirical relationship between C sink and stand age [*Acker et al.*, 2002; *Ryan et al.*, 2004; *Wirth*, 2009; *Hudiburg et al.*, 2009], and extrinsic factors, which reflect the integrated effects of environmental conditions [*Law et al.*, 2002; *Hember et al.*, 2012]. Forest successional dynamics is related with forest age and the successional stages usually covary with age. In most cases, the age response of a C sink consists of a rapid initial increase followed by a gradual decline to a new steady state [*Chen et al.*, 2003; *Hudiburg et al.*, 2009]. Although this pattern is widely supported by chronosequence observations of C stocks [*Thornton et al.*, 2002;

Bond-Lamberty et al., 2004; *Pregitzer and Euskirchen*, 2004; *Gough et al*., 2007; *Yang et al*., 2011] and forest-atmosphere net CO_2 exchange [*Barford et al*., 2001; *Amiro et al*., 2010; *Goulden et al*., 2011], the precise relationship between forest C sink and forest age remains poorly characterized because it varies with spatially heterogeneous climate, terrain, and soil properties [*Williams et al*., 2012; *Kashian et al*., 2013]. A large number of field observation sites are necessary to distinguish the potential impacts of these extrinsic factors.

Several methods are commonly used to estimate the relationship between the C sink and forest age. One basic approach is the chronosequence approach [*Kashian et al*., 2013], which is based on the observations of carefully selected age sequences of forest stands. Based on the field observations (e.g., tree diameter, height, wood increment, age, coarse woody debris, and species), the species-specific allometric equations were used to estimate live and dead biomass stores, net primary productivity (NPP), and mortality [*Hudiburg et al*., 2009]. The plot locations were usually selected using a hierarchical random sampling design based on climate, forest type, and age [*Law et al*., 2006]. However, at the biome level, this approach is inevitably limited by the cost of establishing the many replicate chronosequences necessary to understand biome variability and the interannual variability caused by short-term climatic variability [*Pregitzer and Euskirchen*, 2004].

Another method is the eddy covariance method [*Baldocchi et al*., 2001; *Baldocchi*, 2008], which uses flux towers to monitor and quantify net C exchange between forests and atmosphere and then build the statistical relationship between C sink and age [*Peichl et al*., 2010; *Coursolle et al*., 2012; *Baldocchi*, 2008]. For example, *Yu et al*. [2014] built a NEP-age statistical model based on 34 forest sites of net C exchange observation in the East Asian monsoon region and found that 48.7% variation in observed NEP could be interpreted by forest age. However, the number of forest flux towers is quite small, and the distribution of observation sites is quite uneven around the world. For instance, there are only two evergreen needle-leaved forest sites located in China [*Yu et al*., 2013]. Therefore, the potential impacts of local environmental factors, such as terrain and soil properties, may be high [*Peichl et al*., 2010]. In addition, as the observed value from flux tower is the net C exchange between atmosphere and ecosystem that contains all components of vegetation, litter, and soil carbon pools [*Baldocchi et al*., 2001], its observation alone was impossible to directly estimate the relative contributions of carbon sinks for vegetation and soil pools. As a result, the observations from flux towers were usually used in conjunction with ecosystem models or biometric data and remote sensing to improve the modeled carbon fluxes [*Baldocchi*, 2008].

Process-based models represent another method used to simulate the age-related C sink or fluxes [*Williams et al*., 2012; *Raymond and McKenzie*, 2013]. Ecosystem C sink can be characterized in models by two sets of parameters related to C influx, residence time, and state variables of pool sizes at a given time [*Luo and Weng*, 2011]. The magnitude of C pool at steady state is determined by its C influx and residence time [*Carvalhais et al*., 2014]. When the modeled pool sizes at the time are below the steady state pool sizes, forests sequester C. The difference between the steady state pool sizes and modeled pool sizes at a given time is the sink capacity, or disequilibrium [*Luo and Weng*, 2011]. Thus, to simulate age-dependent forest C sink, it is essential to not only estimate C influx and residence time but also the age-dependent parameters (e.g., maximum of light-use efficiency).

Data assimilation is currently a potential approach to quantify the dynamic disequilibrium (i.e., age-dependent C sink) of the terrestrial carbon cycle [*Luo et al*., 2011; *Luo and Weng*, 2011]. It assimilates multiple sources of information, such as ground-based field observations, remote sensing-based satellite monitoring, and mechanistic process models together to estimate C influx, residence times, and the disequilibrium [*Raupach et al*., 2005; *Wang et al*., 2009; *Luo et al*., 2011; *Kuppel et al*., 2012]. Our previous study indicated that the widely available but spatially isolated biometric observations (i.e., NPP, biomass, litter, and soil organic carbon) can be effectively integrated to estimate the magnitudes of C sinks at nonsteady state [*Zhou et al*., 2013]. Biometric observations are much easier to measure than NEE observation by flux towers and thus available at many geographic regions with much rich site information. Based on the samples of age-dependent biometric observations, the age-dependent C sink can be inversely estimated.

To better simulate the dynamics of carbon cycle in a process-based model, we need to explicitly express the quantitative relationships (e.g., what kind of function form) between forest age and the age-related fluxes and parameters. As a result, one of the main objectives in the present study was to inversely estimate these feasible age-dependent relationships using the age-specific observation subsets and then to build suitable statistical relationships among them. Specifically, we aim to inversely estimate a quantitative relationship

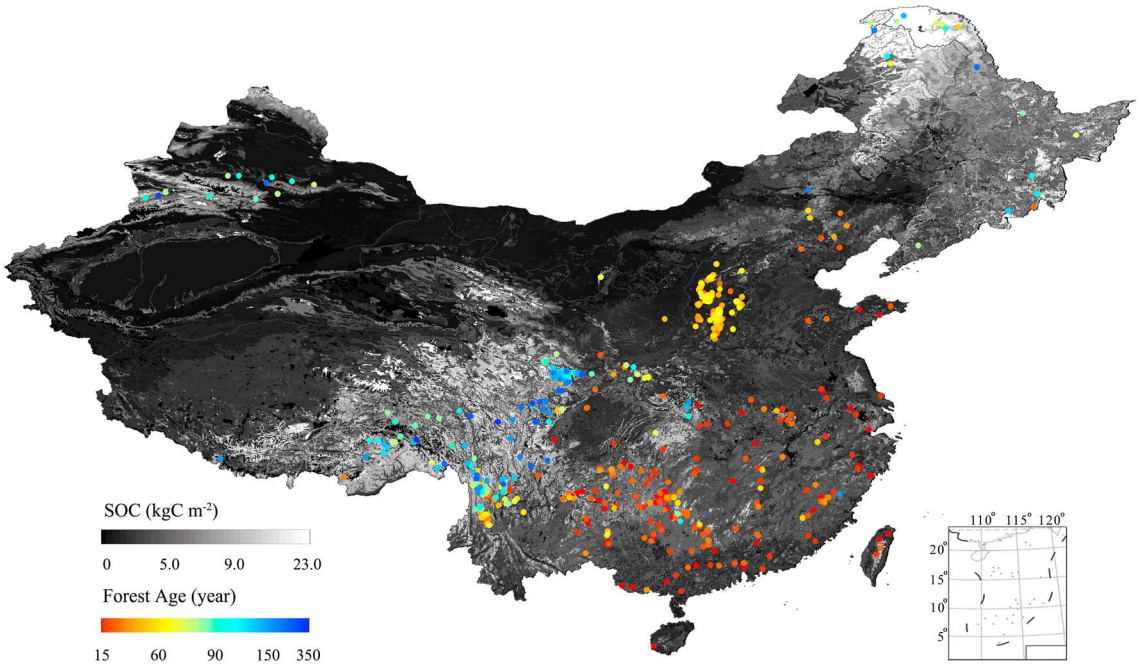

Figure 1. The observations of NPP, biomass, and SOC that used to inversely estimate the model parameters. There are extensively distributed 588 field sites for forest biometrical observations (i.e., NPP and biomass in leaves, stems, and roots), which comes from the literature by *Luo* [1996]. The site-related SOC were extracted from a spatially explicit SOC map with 1 km spatial resolution, which generated by *Shangguan et al.* [2013] from 8979 soil profiles.

between the magnitude of the C sink and forest age from multiple sources of data and to address two scientific problems for evergreen needle-leaved forests in China: (1) the temporal dynamics of ecosystem C sink, i.e., the quantitative relationship between the forest C sink (i.e., the magnitude and efficiency) and forest age, and (2) the differences in the C sink rate and duration between vegetation and soil pools and their implications for C sink evaluation and long-term forest C management.

2. Data and Methods

2.1. Assimilated Data

Eleven data sets related with forest age were used in this study to estimate age-related C sink parameters and to build the statistical relationship between ecosystem C sink and age. These data sets included three age-related NPP data sets (i.e., NPP in leaves, stems, and roots), each containing 588 data points [*Luo*, 1996], five age-related biomass data sets (i.e., biomass of leaves, stems, and roots in three soil layers), each containing 588 data points [*Luo*, 1996], and three SOC data sets for the three soil layers, originating from the spatially explicit SOC map with 1 km spatial resolution, which was generated by *Shangguan et al.* [2013] from 8979 soil profiles. There are two main reasons for us to use this gridded SOC data set. First, it contained the most extensive observation sites and therefore could better represent spatial heterogeneity. Second, this data set was developed for land surface modeling and therefore contains comprehensive information on physical and chemical attributes of soils and on vertical distribution that meets the soil submodel scheme (i.e., 0–100 cm). Because information on forest age was unavailable for most of the soil profiles, the spatial grids around the locations of NPP and biomass observations were used to represent the forest age-related SOC. That is, we first obtained latitude and longitude values from NPP and biomass observation sites where forest ages were available and then extracted the corresponding SOC values from 9×9 grids centered on these sites (Figure 1). We used the means of the 9×9 grids to represent the SOC of corresponding sites, instead of one grid per site location, to diminish possible errors in the spatial data processes. The detailed distribution of these forest age-related site observations (NPP and biomass) and their corresponding SOC map are illustrated in Figure 1, and the summarization of data sets list in Table 1.

To estimate age-independent baseline C residence times for litter and SOC pools under steady state assumption, 27 litter and 15 SOC observations at the old forest site were collected from the literature

Table 1. Summarization of Field Observations Used for Parameters Estimation

Data Type	Unit	Minimum	Maximum	Mean	Standard Deviation	Source
NPP in leaves	kg C m^{-2} yr^{-1}	0.0380	0.6626	0.2093	0.1151	*Luo* [1996]
NPP in stems	kg C m^{-2} yr^{-1}	0.0442	1.0778	0.2488	0.159	*Luo* [1996]
NPP in roots	kg C m^{-2} yr^{-1}	0.0052	0.209	0.0491	0.034	*Luo* [1996]
Biomass of leaves	kg C m^{-2}	0.0974	1.8744	0.4801	0.2429	*Luo* [1996]
Biomass of stem	kg C m^{-2}	0.6303	66.4544	5.7471	4.7393	*Luo* [1996]
Biomass of root (0–20 cm)[a]	kg C m^{-2}	0.0945	2.8459	0.5551	0.415	*Luo* [1996]
Biomass of root (20–50 cm)[a]	kg C m^{-2}	0.0675	2.0320	0.3963	0.2963	*Luo* [1996]
Biomass of root (50–100 cm)[a]	kg C m^{-2}	0.0353	1.0637	0.2075	0.1551	*Luo* [1996]
SOC (0–20 cm)	kg C m^{-2}	0.7455	18.3359	4.4625	2.6494	*Shangguan et al.* [2013]
SOC (20–50 cm)	kg C m^{-2}	0.6753	15.5689	2.9303	1.4433	*Shangguan et al.* [2013]
SOC (50–100 cm)	kg C m^{-2}	0.6941	8.1891	2.2743	0.858	*Shangguan et al.* [2013]
Flux tower observation[b]	kg C m^{-2} yr^{-1}	0.3130	0.4880	-	-	*Yu et al.* [2013]

[a]Estimated with root biomass [*Luo*, 1996] and root distribution model [*Jackson et al.*, 1996].
[b]Two flux tower sites of evergreen needle-leaved forest (QYZ and HT), used only for validation.

(reference *Zhou et al.* [2013]). In addition, the flux tower observation data of net ecosystem exchange in ChinaFLUX [*Yu et al.*, 2013] were collected at two sites of evergreen needle-leaved forests, Qianyezhou (QYZ, latitude 26.73°, longitude 115.02°, forest age 21 years) and Huitong (HT, latitude 26.83°, longitude 109.75°, forest age 13 years). We used these data for verification and not for parameter estimation.

2.2. Model Drivers

To drive the model, this study used spatially explicit remote sensing and GIS data sets, including (1) the advanced very high resolution radiometer/normalized difference vegetation index (AVHRR-NDVI) continental subsets of 8 km spatial resolution from 1982 to 2000 available from the Global Inventory Modeling and Mapping Studies [*Tucker et al.*, 2004]. As one of the main objectives was to optimize and evaluate model parameters, we used the original satellite-derived NDVI data set instead of the NDVI-based fPAR products to model the NPP. (2) GIS data sets of monthly solar radiation, temperature, and precipitation from the China Meteorological Data Sharing Service System [*China Meteorological Administration*, 2015], which are site observations from 1982 to 2000 and we interpolated them using kriging method to produce gridded images with the same spatial resolution (i.e., 8 km) as AVHRR-NDVI. And (3) a 1:14,000,000 soil texture map of China.

All of those auxiliary data sets were resampled to a common geographic (latitude/longitude) projection and spatial resolution (0.08°) using Bilinear Interpolation in ERDAS Imagine software (Leica Geosystems Geospatial Imaging, LLC). Most of the ground-based observations of NPP and biomass were measured during the 1980s and 1990s, so we applied the same time period of NDVI and climate factors and used their multiyear monthly means for 1982–2000 to model NPP and biomass and compare with ground-based observations. The model simulates the monthly NPP based on monthly NDVI and climate data, which were then summed to yearly total NPP before estimation of the parameters.

2.3. Model

The process-based Terrestrial ECOsystem Regional (TECO-R) model [*Zhou and Luo*, 2008; *Zhou et al.*, 2010, 2013] was used in the data assimilation to synthesize information from the model, field observations, and spatially explicit satellite data. The TECO-R model contains three sequential submodels that determine ecosystem C input (i.e., net primary production), the C allocation of NPP to different vegetation C pools (i.e., leaves, stems, and roots) and the turnover and decomposition of the litter and soil organic C. TECO-R uses a light-use efficiency (LUE) scheme of the CASA model [*Potter et al.*, 1993; *Field et al.*, 1995] to simulate the spatially specific NPP pattern at the regional scale. The NPP is determined from the satellite-based normalized difference vegetation index (NDVI) and climate driving factors. The estimated NPP is allocated to different vegetation C pools (leaves, stem, and roots) based on NPP allocation coefficients (α_L, α_W, α_R, ξ_{R1}, ξ_{R2}, and ξ_{R3}) (Table 2). Then, the C enters carbon pools of the litter and soil organic carbon and is eventually released from the ecosystem though heterotrophic respiration. The model structure is illustrated in Figure 2, and the key parameters related to this study are listed in Table 2. Details about the TECO-R model's structure, parameters, and processes were described in *Zhou and Luo* [2008] and *Zhou et al.* [2013].

Table 2. Definitions of Parameters in TECO-R Model and the Lower and Upper Limits

Symbol	Definition	Unit	Lower Limit	Upper limit
ε^*	Maximum light-use efficiency	g C MJ^{-1}	0.0	2.76
α_L	Allocation of NPP to leaves	Dimensionless	0.0	1.0
α_W	Allocation of NPP to wood	Dimensionless	0.0	1.0
α_R	Allocation of NPP to roots	Dimensionless	0.0	1.0
ξ_{R1}	Allocation proportion of NPP for roots(0–20 cm)	Dimensionless	0.0	1.0
ξ_{R2}	Allocation proportion of NPP for roots(20–50 cm)	Dimensionless	0.0	1.0
ξ_{R3}	Allocation proportion of NPP for roots(50–100 cm)	Dimensionless	0.0	1.0
θ_F	Carbon partitioning coefficient of the fine litter pool	Dimensionless	0.0	0.5
θ_C	Carbon partitioning coefficient of coarse litter pool	Dimensionless	0.0	0.5
θ_{S1}	Carbon partitioning coefficient of SOC (0–20 cm)	Dimensionless	0.0	0.1
θ_{S2}	Carbon partitioning coefficient of SOC (20–50 cm)	Dimensionless	0.0	0.1
η	Fraction of mechanical breakdown for coarse litter pool	Dimensionless	0.0	0.1
τ_L	Site specific carbon residence time of leaves	Year	0.0	10.0
τ_W	Site specific carbon residence time of wood	Year	0.0	500.0
τ_{R1}	Site specific carbon residence time of roots (0–20 cm)	Year	0.0	10.0
τ_{R2}	Site specific carbon residence time of roots (20–50 cm)	Year	0.0	20.0
τ_{R3}	Site specific carbon residence time of roots (50–100 cm)	Year	0.0	50.0
τ_F^*	Baseline residence time of fine litter	Year	0.0	10.0
τ_C^*	Baseline residence time of coarse litter	Year	0.0	50.0
τ_{S1}^*	Baseline residence time of SOC (0–20 cm)	Year	0.0	100.0
τ_{S2}^*	Baseline residence time of SOC (20–50 cm)	Year	0.0	250.0
τ_{S3}^*	Baseline residence time of SOC (50–100 cm)	Year	0.0	500.0
Δ_L	Net carbon gain or release for leaf pool	g C m^{-2} yr^{-1}	−200	200
Δ_W	Net carbon gain or release for wood pool	g C m^{-2} yr^{-1}	−1000	1000
Δ_{R1}	Net carbon gain or release for roots (0–20 cm)	g C m^{-2} yr^{-1}	−200	200
Δ_{R2}	Net carbon gain or release for roots (20–50 cm)	g C m^{-2} yr^{-1}	−200	200
Δ_{R3}	Net carbon gain or release for roots (50–100 cm)	g C m^{-2} yr^{-1}	−200	200
Δ_F	Net carbon gain or release for fine litter pool	g C m^{-2} yr^{-1}	−200	200
Δ_C	Net carbon gain or release for coarse litter pool	g C m^{-2} yr^{-1}	−200	200
Δ_{S1}	Net carbon gain or release for SOC pool (0–20 cm)	g C m^{-2} yr^{-1}	−500	500
Δ_{S2}	Net carbon gain or release for SOC pool (20–50 cm)	g C m^{-2} yr^{-1}	−500	500
Δ_{S3}	Net carbon gain or release for SOC pool (50–100 cm)	g C m^{-2} yr^{-1}	−500	500

As optimization of different parameter subsets against different data streams helps to counteract the problem of transfer of model uncertainty [*Wutzler and Carvalhais*, 2014], we divided the model parameters into three groups to effectively estimate age-dependent forest C sink. The first group ($\mathbf{P_0}$) defines carbon cycle at a steady state forest ecosystem, including C residence times of 10 pools (i.e., $\tau_L, \tau_W, \tau_{R_1}, \tau_{R_2}, \tau_{R_3}, \tau_F^*, \tau_C^*, \tau_{S_1}^*, \tau_{S_2}^*$, and $\tau_{S_3}^*$) and five related partition coefficients among C pools (i.e., $\theta_F, \theta_C, \eta, \theta_{S_1}$, and θ_{S_2}), which define the proportions of C entering into the next pools. These parameters are commonly set as constants in process-based models. The second group ($\mathbf{P_1}$) includes the potential maximum light-use efficiency and allocation coefficients of NPP among different live biomass pools (i.e., $\varepsilon^*, \alpha_L, \alpha_W$, and α_R), which are age dependent and control input of C into various plant pools. The third group of parameters ($\mathbf{P_2}$) includes 10 nonsteady state C sink parameters (i.e., $\Delta_L, \Delta_W, \Delta_{R_1}, \Delta_{R_2}, \Delta_{R_3}, \Delta_C, \Delta_F, \Delta_{S_1}, \Delta_{S_2}$, and Δ_{S_3}), which define the net C gain or release for corresponding pools, and 3 NPP allocation coefficients to roots (i.e., ξ_{R1}, ξ_{R2}, and ξ_{R3}). Those parameters are also age dependent and related to both C input parameters ($\mathbf{P_1}$) and output parameters ($\mathbf{P_0}$). The three root allocation coefficients were included in $\mathbf{P_2}$ due to the absence of NPP observations for roots in different soil layers. The detailed algorithms to describe the relationships of modeled C fluxes and pools with these parameters were presented in *Zhou et al.* [2013].

2.4. Stepwise Data Assimilation: General Procedure

The stepwise approach is developed from the two-step data assimilation method [*Zhou et al.*, 2013]. The reason we used a stepwise data assimilation approach, instead of a one-step approach, is based on the consideration that the number of parameters constrained by the observation data sets is limited, typically from several parameters to less than 20 parameters [*Wang et al.*, 2001; *Braswell et al.*, 2005; *Xu et al.*, 2006; *Yuan et al.*, 2012]. If we use a one-step approach, 32 model parameters would need to be simultaneously estimated; and it is difficult to constrain all those parameters [*Zhou et al.*, 2013]. To illustrate the uncertainties

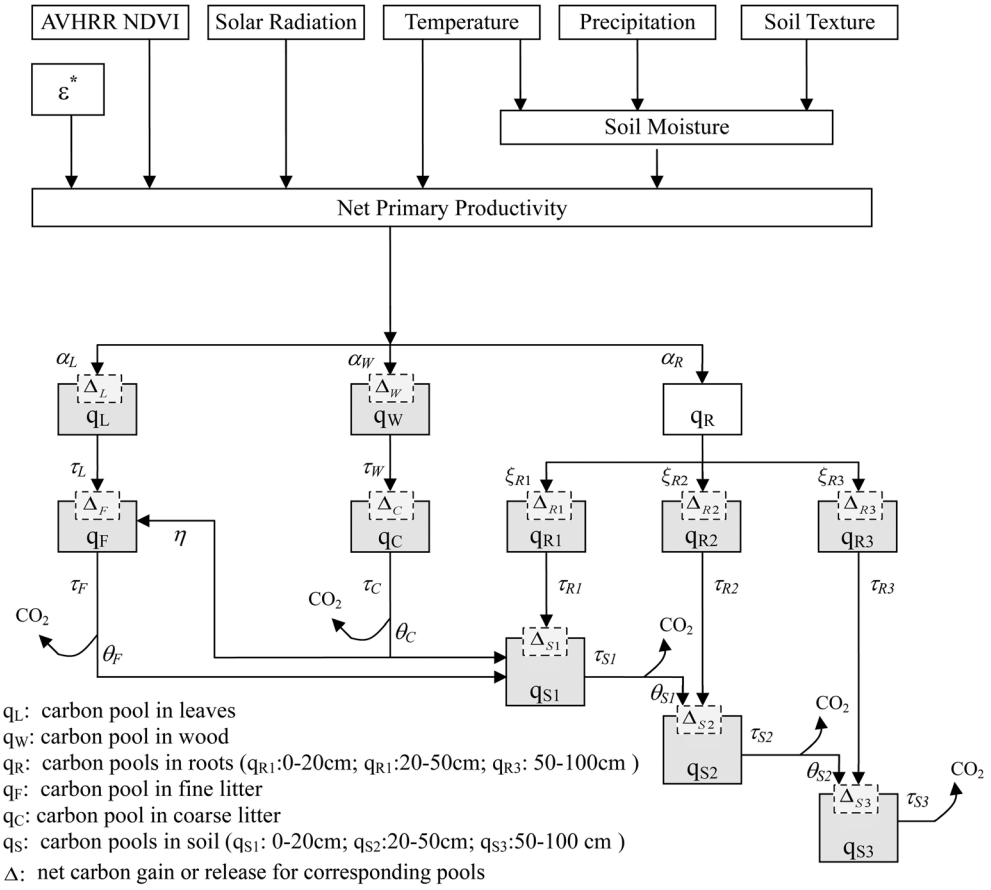

Figure 2. The structure of the Terrestrial ECOsystem Regional (TECO-R) model and its key parameters. NPP is modeled by the light-use efficiency model, and it allocated to plant tissues on the basis of allocation coefficients. Plant tissues enter into fine litter, coarse litter, and soil organic carbon pools through litterfall. Decomposed litter releases part of the carbon to the atmosphere, and the rest transfers into the soil. For the steady state, the carbon sink parameters (i.e., net carbon gain/release) equal zeros. For the nonsteady state, however, the carbon sink parameters were inversely estimated to match the observed NPP and carbon pools in vegetation and SOC.

of parameters, the histograms of the optimized 32 parameters were produced. Specifically, we ran the genetic algorithm 500 times and obtained 500 optimal parameters, each representing a combination of parameters of similar cost function value, from which we could judge whether and what parameters were well constrained by the observations (Figures S1–S3 in the supporting information).

In this study, we use a stochastic sampling from observation data sets to generate samples of age-related observations, from which the forest age-related C sink parameters were inversely estimated from different samples with a genetic algorithm [*Zhou and Luo*, 2008]. Then we build a statistical relationship between estimated C sink and forest age. The detailed flow chart illustrated in Figure 3.

Step 1. Estimating the age-independent parameters of C residence times for individual pools ($\mathbf{P_0}$) from field observations (NPP, biomass, litter, and SOC) of old forests (age > 100 years) under the steady state assumption by minimizing the following cost function (reference *Zhou et al.* [2013]):

$$J = \sum_{m=1}^{12} \lambda_m \left\{ \sum_{n=1}^{N_m} [y_{nm} - \hat{y}_{nm}(x_n, \mathbf{P_0}, \mathbf{a})]^2 \right\}, \quad (1)$$

where y_{nm} is the nth observed data point in the mth data set; $\hat{y}_{nm}(x_n, \mathbf{P_0}, \mathbf{a})$ is the modeled value that corresponds to the observation y_{nm}; N_m is the total number of data points in the mth data set; x_n is an auxiliary forcing vector that includes NDVI, solar radiation, air temperature, precipitation, and soil texture, in a spatial grid where the nth observation was measured; **a** is a vector consisting of seven old

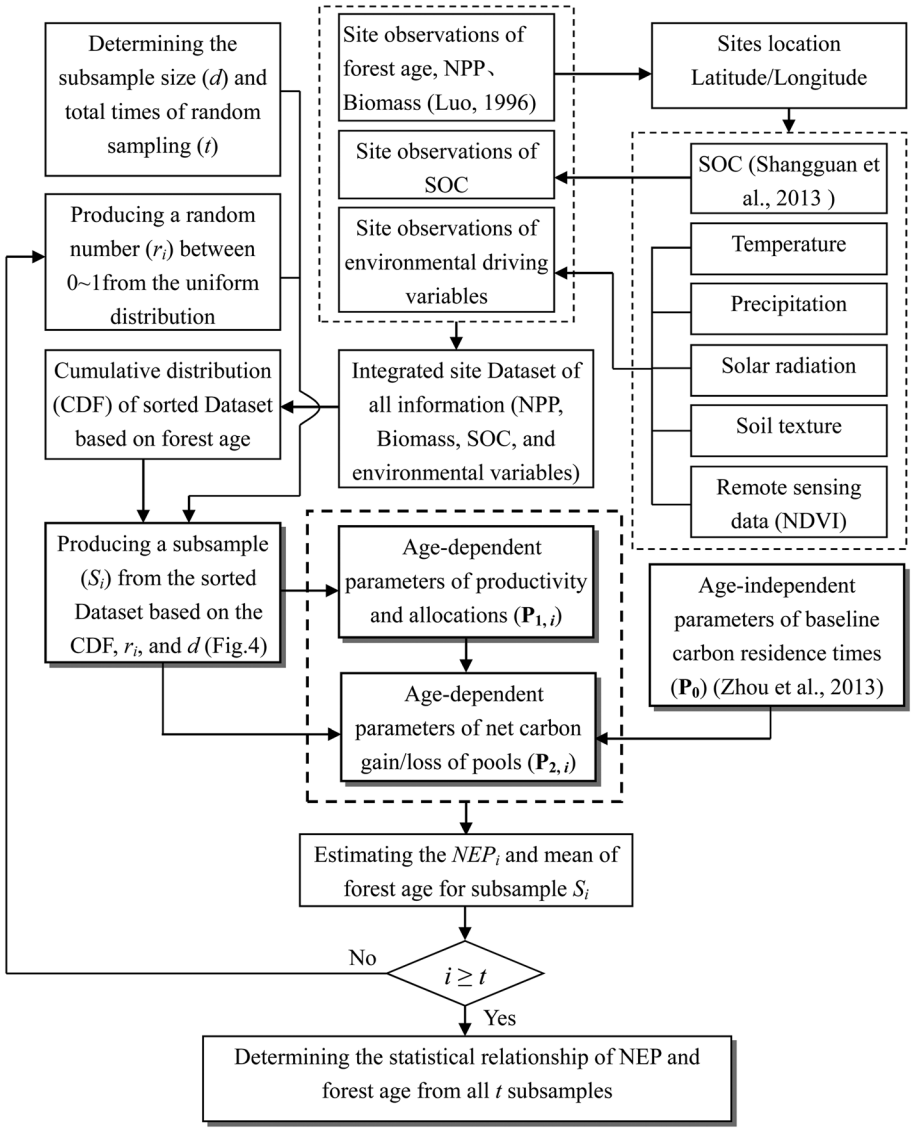

Figure 3. Flow chart of stepwise data assimilation.

forest-related parameters: $\mathbf{a} = \{\varepsilon^*, \alpha_L, \alpha_W, \alpha_R, \xi_{R1}, \xi_{R2}, \xi_{R3}\}$; and λ_m is a weighting factor of the partial cost function, which is inversely proportional to the variance of each data set [*Luo et al.*, 2003; *Zhou and Luo*, 2008]. These estimated values of $\mathbf{P_0}$ were used as known age-independent constants in the rest of the data assimilation.

Step 2. Establishing data sets of age-related variables, such as NPP, biomass, SOC, and relevant driving variables (i.e., NDVI, temperature, precipitation, solar radiation, and soil texture) based on site observations.

Step 3. Randomly sampling a fraction (e.g., 20%) of data of the age-dependent variables from the data sets (reference Figure 4) with four substeps. One objective of this study was to derive a suitable statistical model between NEP and forest age. Considering that NEP is related to both forest age and environmental factors (e.g., climate and terrain) that have a high spatial heterogeneity and potentially impact the inference of NEP-age relationship, a key step was to diminish the interference of site-specific environmental factors. The observation subset, which had similar forest age but different environmental factors, was suitable to eliminate the interference of environmental factors, as the mean of multiple sites tends to weaken the potential impact of a single site and highlight the common age effect of multiple sites.

Step 3.1. Determining subsample size d ($d = 0.2$) and total times of random sampling ($t = 500$).

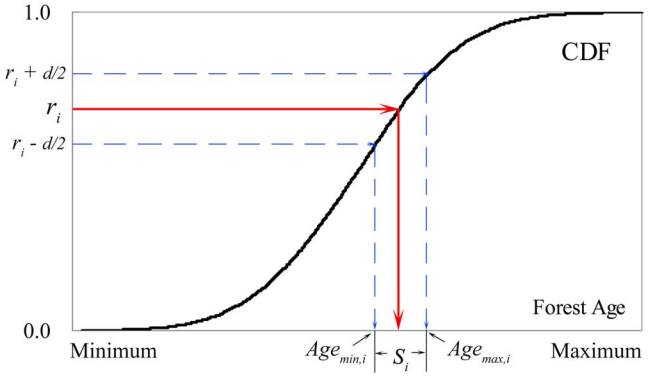

Figure 4. Schematic diagram for stochastic sampling of subsample with similar forest age.

Step 3.2. Sorting the data sets based on forest age to build a cumulative distribution function (CDF). As each site in data set of *Luo* [1996] simultaneously contains the information of forest age, NPP, and biomass, we just need one CDF.

Step 3.3. Producing a random number (r_i) between 0 and 1 from a uniform distribution.

Step 3.4. Producing an age-related subsample S_i from CDF, d, and r_i (reference Figure 4). The low bound ($Age_{min,\,i}$) and upper bound ($Age_{max,\,i}$) correspond with the random numbers $r_i - d/2$ and $r_i + d/2$. If the value of $r_i - d/2 < 0$ or $r_i + d/2 > 1$, then the value of $Age_{min,\,i}$ is assigned to the minimum or $Age_{max,\,i}$ is assigned to the maximum of the observed data sets. In this situation, the size of subsample is between $d/2$ and d.

Step 4. Estimating the nonsteady state C sink parameters from the subsample S_i with the stepwise data assimilation.

Step 4.1. Estimating the age-dependent parameters of productivity and its allocation parameters ($\mathbf{P_{1,\,i}}$) from the subsample S_i by minimizing the cost function J' as

$$J' = \sum_{u=1}^{3} \lambda_u \left\{ \sum_{n=1}^{N_u} [y_{nu} - \hat{y}_{nu}(x_n, \mathbf{P_1})]^2 \right\}, \tag{2}$$

where $\hat{y}_{nu}(x_n, \mathbf{P}_1)$ is the modeled value that corresponds to the observation y_{nu} of subsample S_i, N_u is the observation number of subsample S_i, and λ_u is a weighting factor, which is inversely proportional to the variance of each data set. Accurately simulating the primary productivity of the ecosystem is crucial because errors in simulated NPP propagate through the model to introduce additional errors in simulated biomass and other fluxes [*Schaefer et al.*, 2012; *He et al.*, 2014].

Step 4.2. Estimating the age-dependent C sink parameters of pools ($\mathbf{P_{2,\,i}}$) under the nonsteady state condition, from the same subsample S_i and the known parameters $\mathbf{P_0}$ and $\mathbf{P_{1,\,i}}$ by minimizing the cost function J'' as

$$J'' = \sum_{v=1}^{8} \lambda_v \left\{ \sum_{n=1}^{N_v} [y_{nv} - \hat{y}_{nv}(x_n, \mathbf{P_2})]^2 \right\}, \tag{3}$$

where $\hat{y}_{nv}(x_n, \mathbf{P_2})$ is the modeled biomass or SOC that corresponds to the observation y_{nv} of subsample S_i, N_v is the number of subsample S_i, λ_v is a weighting factor, which is inversely proportional to the variance of each data set. Because the $\mathbf{P_1}$ parameters control the basic C input and the $\mathbf{P_0}$ parameters control the basic C output, the observations of biomass and SOC may well constrain parameters $\mathbf{P_{2,\,i}}$ [*Zhou et al.*, 2013].

Step 4.3. Summarizing the age-dependent ecosystem total C sink (i.e., NEP_i) of the subsample S_i from 10 C sink parameters.

Step 5. Repeating the random sampling and stepwise estimations of nonsteady state parameters (Steps 3.3 to 4.3) 500 times and then determining the statistical relationship between C sink and forest age from all 500 subsamples.

As a genetic algorithm was used in our study, we need to run the model iteratively for each new parameter vector until the optimized one was obtained (Steps 1, 4.1, and 4.2). Considering that too much simulation was required, we applied an analytical solution [*Zhou et al.*, 2013] instead of spin-up, to get the modeled values and compared them with the corresponding observations.

2.5. Sensitivity Analysis of Subsample Size on Parameter Estimation

To assess the potential impacts of sample size (i.e., d value) on the relationship of C sink and age, we performed a sensitivity analysis for different subsample sizes on parameter estimation. We assigned values

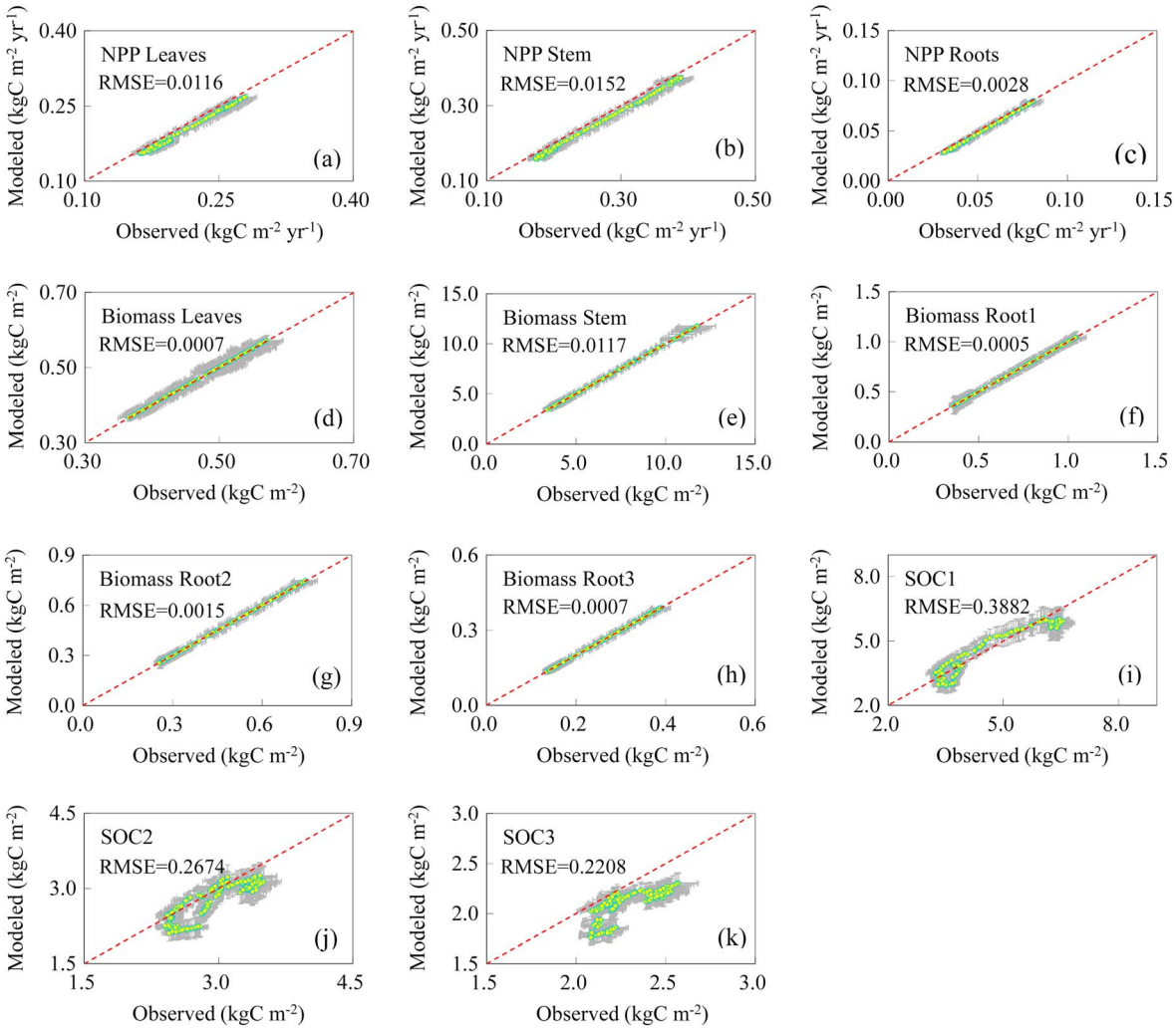

Figure 5. Comparisons between the modeled and observed means (±1 standard error) of random subsamples.

0.025, 0.05, 0.10, 0.20, and 0.30 (i.e., the subsample size is 2.5% to 30% of the total number of observations) to the parameter *d* and then compared the differences in the estimated relationships between C sink and age in five scenarios.

3. Results

3.1. Comparisons Between Modeled and Observed Values

The comparisons indicated that the modeled means of NPP and biomass very closely matched the corresponding observations of subsamples (Figure 5). The good match between observed and modeled biomass pools was mainly due to the nonsteady state scheme, as we added 10 adjustable C sink parameters that would significantly decrease the deviation between modeled and observed value (i.e., through adjusting the values of carbon sink parameters to make the modeled pools match with their observed pools). The previous study of *Carvalhais et al.* [2008] showed that adding one adjustable parameter to relax the constraints of the steady state assumption could lead to a 92% decrease in the normalized average error. These comparisons showed that the estimated optimal model parameters are effective to help fit the model with data of the C fluxes and pools.

The observed and modeled values for soil organic carbon are also matched well, but the goodness of fit is somewhat lower than for NPP and biomass. One possible cause of the relative higher uncertainty of soil carbon estimation is likely due to the higher uncertainties of their related model parameters, such as much

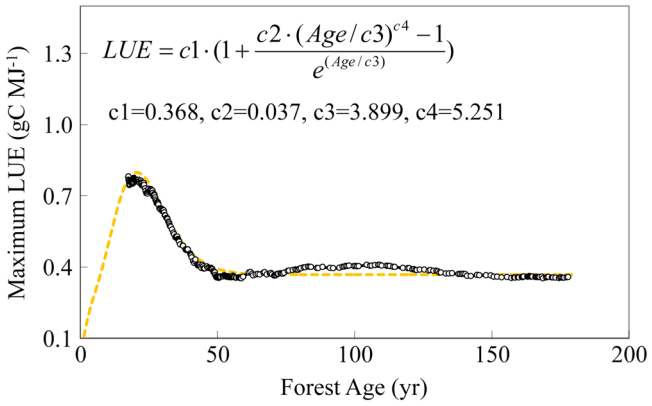

Figure 6. Relationship between maximum light-use efficiency and forest age ($R^2 = 0.99$).

higher variations in the optimal parameters of soil carbon residence time (Figure S1). In addition, change in soil carbon stock is controlled by other processes of the carbon cycle such as photosynthesis, litter fall, and decomposition, and therefore, much more uncertainty is transmitted from upstream processes. The other cause is that the SOC observations were not directly measured at forest sites but were derived from the observation-based map of soil organic carbon [*Shangguan et al.*, 2013], which unavoidably increased the error. Due to the higher spatial heterogeneity and the relative sparse observation sites, the highest uncertainties of the modeled carbon storage and fluxes in current studies were usually related with SOC [*Viscarra Rossel et al.*, 2014; *Tian et al.*, 2015]. To decrease the uncertainty of modeled SOC, not only the complete information (e.g., vertical distribution of SOC) but also the extensive distribution of sites was needed to diminish the potential impacts of its spatial heterogeneity [*Scharlemann et al.*, 2014].

3.2. Age Dependence of Light-Use Efficiency and NPP Allocations

For a certain subsample (S_i), its age-specific parameters and uncertainties could be estimated based on stepwise data assimilation (Figure S3). As a result, the relationship of age dependence of light-use efficiency and NPP allocation could be obtained from a series of subsamples produced by the stochastic sampling. Our study indicated that the parameter of maximum light-use efficiency depends on forest age, with higher light-use capacity for young forests and lower capacity for old forests (Figure 6; $R^2 = 0.99$). The value is the highest at approximately 0.78 g C MJ^{-1} at age 17 years and then decreases rapidly to approximately 0.37 g C MJ^{-1} when forest age exceeds 50 years; it is more constant when age > 50. The changing trend of the inversely estimated maximum light-use efficiency matches well with the theoretical interpretation that foliage of older trees shows lower photosynthetic capacity and lower diurnal assimilation than foliage of younger trees [*Ryan et al.*, 1997], and it is also consistent with the field observations showing that growth efficiency declines along a chronosequence of forest age [*Kashian et al.*, 2013].

Based on a similar data set of NPP field observations, *Zhu et al.* [2006] estimated the maximum light-use efficiencies (ε^*) by a modified least squares function and found that its value was 0.389 g C MJ^{-1} for evergreen needle-leaved forest, similar to our previous estimation of 0.378 g C MJ^{-1} using a genetic algorithm [*Zhou et al.*, 2013]. Similar maximum light-use efficiency of evergreen needle-leaved forest (0.36 g C MJ^{-1}) was found in the conterminous United States [*Zhou and Luo*, 2008]. In this study, we further investigated the age dependence of light-use efficiency and found that ε^* decreased with forest age, with values in the range of 0.352–0.782 g C MJ^{-1}. That is, if the age-related difference in light-use efficiency was ignored, NPP would be underestimated for young forests but overestimated for old forests. *Wang et al.* [2011] also investigated the age dependence of NPP and found that the highest NPP was at age of 13 years, comparable to our estimated 17 years when ε^* was at a maximum.

The results of C allocation among different pools indicate that the ratio of NPP allocated to leaves increases with age, while allocations to stem and roots decrease with age (Figure 7). These results also indicated that C allocation to roots in the top-soil layer (0–20 cm) increases with age. The allocation parameter to roots was constrained partly by the observed SOC, as it affected the modeled SOC and the cost function. The observed SOC data set indicated that the ratio of SOC in lower soil layer decreased with increasing age. The ratio of SOC3 (bottom, 50–100 cm) to SOC1 (top, 0–20 cm) was 0.59 ± 0.05 in young and middle-aged forests (age < 100 years), and this ratio decreased to 0.39 ± 0.01 in old forests (age ≥ 100). The trend of NPP allocation obtained in this study is consistent with the theoretical interpretation that the fraction of assimilation

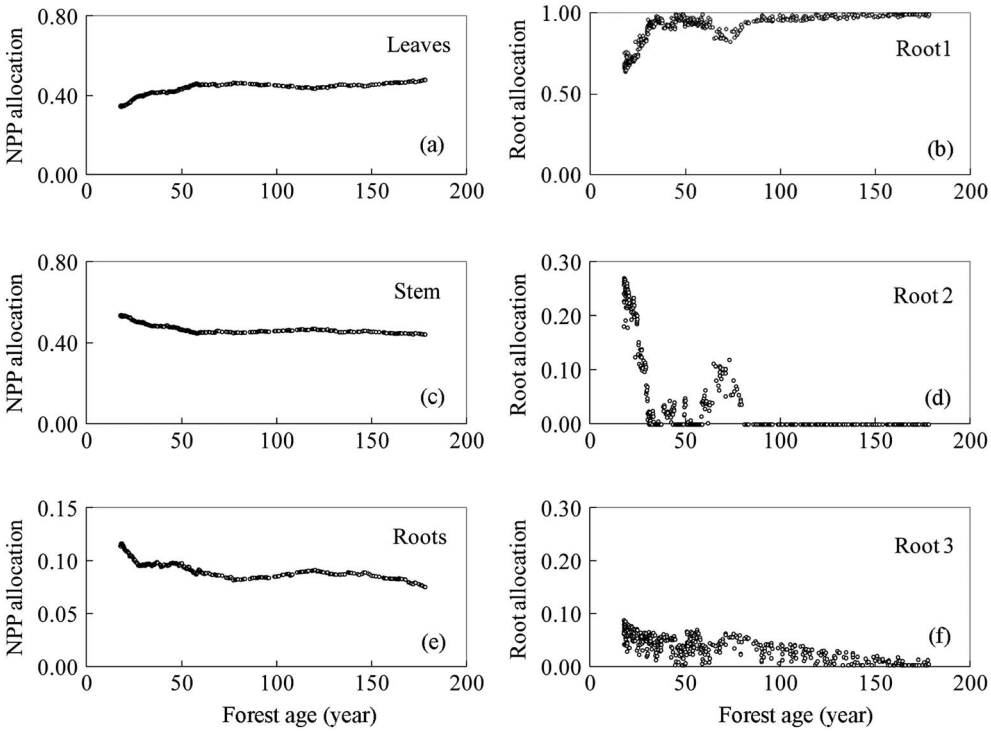

Figure 7. Relationship between NPP allocation coefficients and forest age.

available for wood production declined as woody biomass increased [*Ryan et al*., 1997] and the observation that younger forests dominated by small trees yield more wood [*Caspersen et al*., 2011]. *Litton et al.* [2007] reviewed observation studies of carbon allocation in forest ecosystems and found that carbon allocation varies with stand age with increased allocation to leaves and decreased allocation to roots, which is similar with our results.

Our results indicated that young forests had a relative higher NPP allocation to wood and, accordingly, a relative lower allocation to leaves, which is matched with the trend for field observations [*Luo*, 1996]. Chronosequences using wood increment cores also indicated that young forest stands have a higher

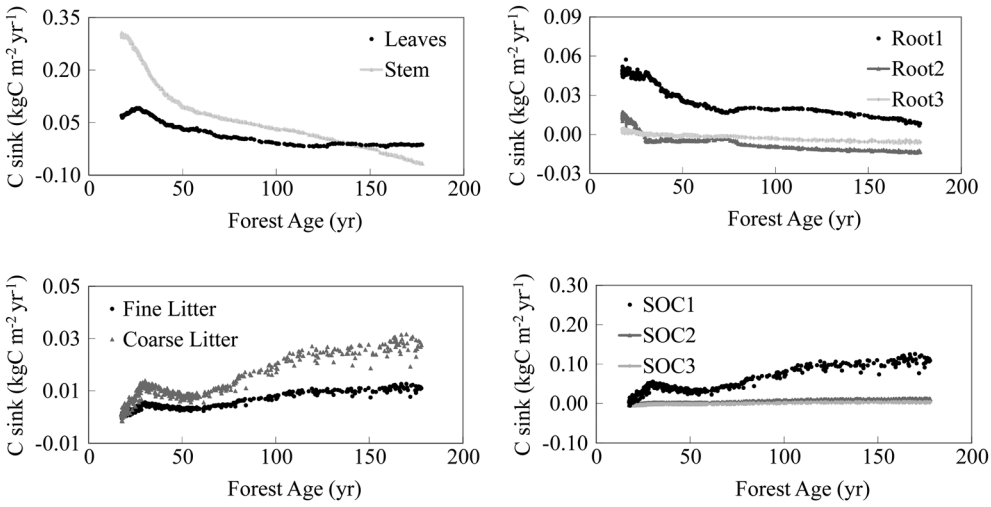

Figure 8. Relationship between carbon sink parameters (i.e., net carbon gain/release) and forest age.

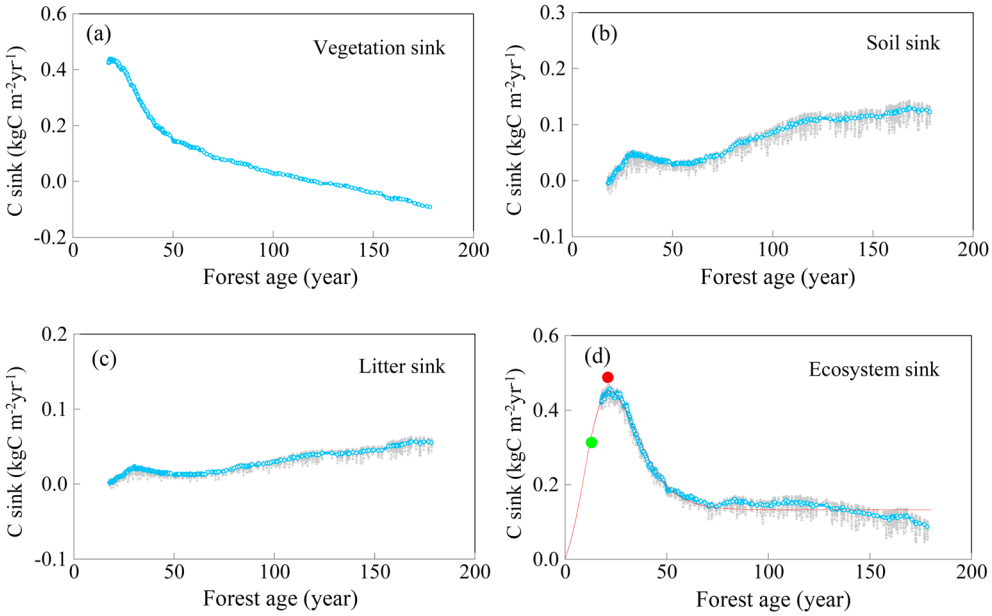

Figure 9. Relationships of vegetation, soil, and ecosystem total carbon sinks and forest age. Each gray point represents an inversed carbon sink from a subsample S_i and a randomly selected parameter vector $\mathbf{P_0}$ in Figure S1. For each S_i, 30 carbon sinks were estimated to reflect the uncertainty caused by the parameters of carbon residence times. Each blue point is the averaged value of 30 estimations for a certain S_i. The red circle is carbon sink observations by flux tower in QYZ (latitude 26.73°, longitude 115.02°, age 21 years), and the green circle is observation in HT (latitude 26.83°, longitude 109.75°, age 13 years) [*Yu et al.*, 2013]. Vegetation carbon sink first increased with forest age and then decreased after peaking at 0.436 kg C m^{-2} yr^{-1}. Soil carbon sink, however, increased continuously with forest age. The estimated ecosystem carbon sink (i.e., NEP) showed a good statistical relationship with forest age: $\mathrm{NEP(Age)} = 0.1323 \cdot \left(1 + \frac{1.0642 \cdot (\mathrm{Age}/6.3342)^{3.4550} - 1}{e^{(\mathrm{Age}/6.3342)}}\right)$.

aboveground wood production than mature forests [*Law et al.*, 2004]. The relatively higher values of light-use efficiency and C allocation to wood give young forests a significantly higher C sink potential.

3.3. Age Dependence of Carbon Sink Parameters

The parameters of C sink (i.e., magnitude of net C gain/release) for different pools are also related with forest ages (Figure 8). The C sink parameter for the leaf pool first increases with age, peaks at 0.092 kg C m^{-2} yr^{-1} at age 27, and then decreases toward 0. The C sink parameters for stem and roots have similar age-dependent patterns. The C sink parameters for the soil and litter pools have a different age-dependent pattern. In general, they increase with forest age but peak at an age near 30 years, three years later than the maximum for the vegetation C sink parameters. For young forest (age $<$ 20 years), soil acts as a C source and after that becomes a C sink with the intensity increasing with age. Similar trends were found in boreal forests where C storage deceased with age for forest age $<$ 10 years and then increased with age [*Chen and Shrestha*, 2012] and in hardwood forests where SOC stock declined with age for forest age $<$ 20 years [*Covington*, 1981].

3.4. Age Dependence of Ecosystem Carbon Sink

The dynamics of vegetation, soil, and the total ecosystem C sink are illustrated in Figure 9. For a subsample (i.e., S_i), we randomly selected 30 parameter vectors of $\mathbf{P_0}$ from Figure S1 and then estimated 30 parameter vectors of $\mathbf{P_2}$, from which the means and uncertainties of C sinks for vegetation, soil, and the whole ecosystem caused by parameters $\mathbf{P_0}$ could be derived. The result indicated that the magnitude of uncertainty for ecosystem carbon sink did not apparently change with forest age, which implied that the observations of different ages were satisfactory to constrain the parameters.

The dynamic patterns of C sink differ between vegetation and soil. The vegetation C sink first increases with forest age, peaks at 0.436 kg C m^{-2} yr^{-1}, and then decreases. Soil C sink, however, increases continuously with forest age, but with a slight decrease between 30 and 50 years due to the rapid decrease of NPP. The age of 20 years is a turning point of soil C uptake, before which soil acts as a C source.

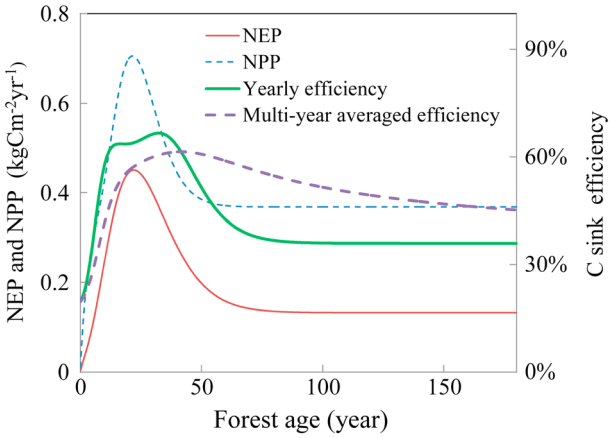

Figure 10. Age dependency of carbon sink efficiency (%) and forest age. The carbon sink efficiency is the ratio of carbon sink and NPP [i.e., carbon sink per unit NPP, *Fang et al.*, 2007]. The carbon sink efficiency for China's evergreen needle-leaved forests changes with forest age, which first increases and then decreases with age, with the highest carbon sink efficiency of about 60% that occurs in young and half-mature forests of ages between 11 and 43 years.

The estimated ecosystem C sink (i.e., NEP) shows a good relationship with forest age (Figure 9) and can be expressed by a nonlinear equation:

$$\mathrm{NEP}(\mathrm{Age}) = a \cdot \left(1 + \frac{b \cdot (\mathrm{Age}/c)^d - 1}{e^{(\mathrm{Age}/c)}}\right), \quad (4)$$

where parameters *a*–*d* are 0.132, 1.064, 6.334, and 3.455, respectively, and the coefficient of determination (R^2) is 0.987. As forest age increases, the ecosystem C sink increases rapidly and peaks at 0.451 kg C m^{-2} yr^{-1}, ranging from 0.421 to 0.465 kg C m^{-2} yr^{-1}, near the age of 22 years before gradually decreasing. The fluxes observed C sink in QYZ (latitude 26.73°, longitude 115.02°, age 21 years) and HT (latitude 26.83°, longitude 109.75°, age 13 year) are 0.488 ± 0.052 and 0.313 kg C m^{-2} yr^{-1}, respectively [*Yu et al.*, 2013], similar to our estimated C sink of 0.449 kg C m^{-2} yr^{-1} at age 21 and 0.332 kg C m^{-2} yr^{-1} at age 13.

The dynamics of the vegetation, soil, and ecosystem C sinks in Figure 9 indicated that the absorbed C is mainly stored in vegetation pools when the forest age is less than 50 years. After that, C is mainly stored in the soil and litter pools. The distinct roles for vegetation and soil pools at different forest ages indicate that long-term forest management tends to increase the soil C sink while short-term afforestation and reforestation mainly affects C sink in vegetation pools.

3.5. Age Dependence of Ecosystem Carbon Sink Efficiency

Although net primary production (NPP) is an input to drive ecosystem C sink, the magnitude of the ecosystem C sink (i.e., NEP) depends on a balance between C input (i.e., NPP) and C output (i.e., heterotrophic respiration

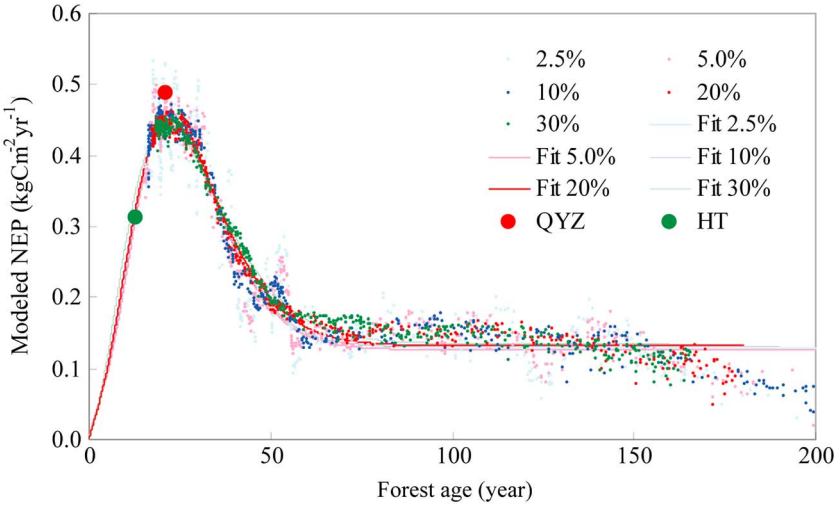

Figure 11. Sensitivities of the estimated relationship of carbon sink and forest age with different size of subsamples. Although a large sample tends to weaken the influences of site-specific geographic factors (e.g., climate, terrain, and soil properties) and then provide a smoother scatterplot than those from smaller samples, the fundamental statistical relationship between carbon sink and forest age is little impacted by the sample size.

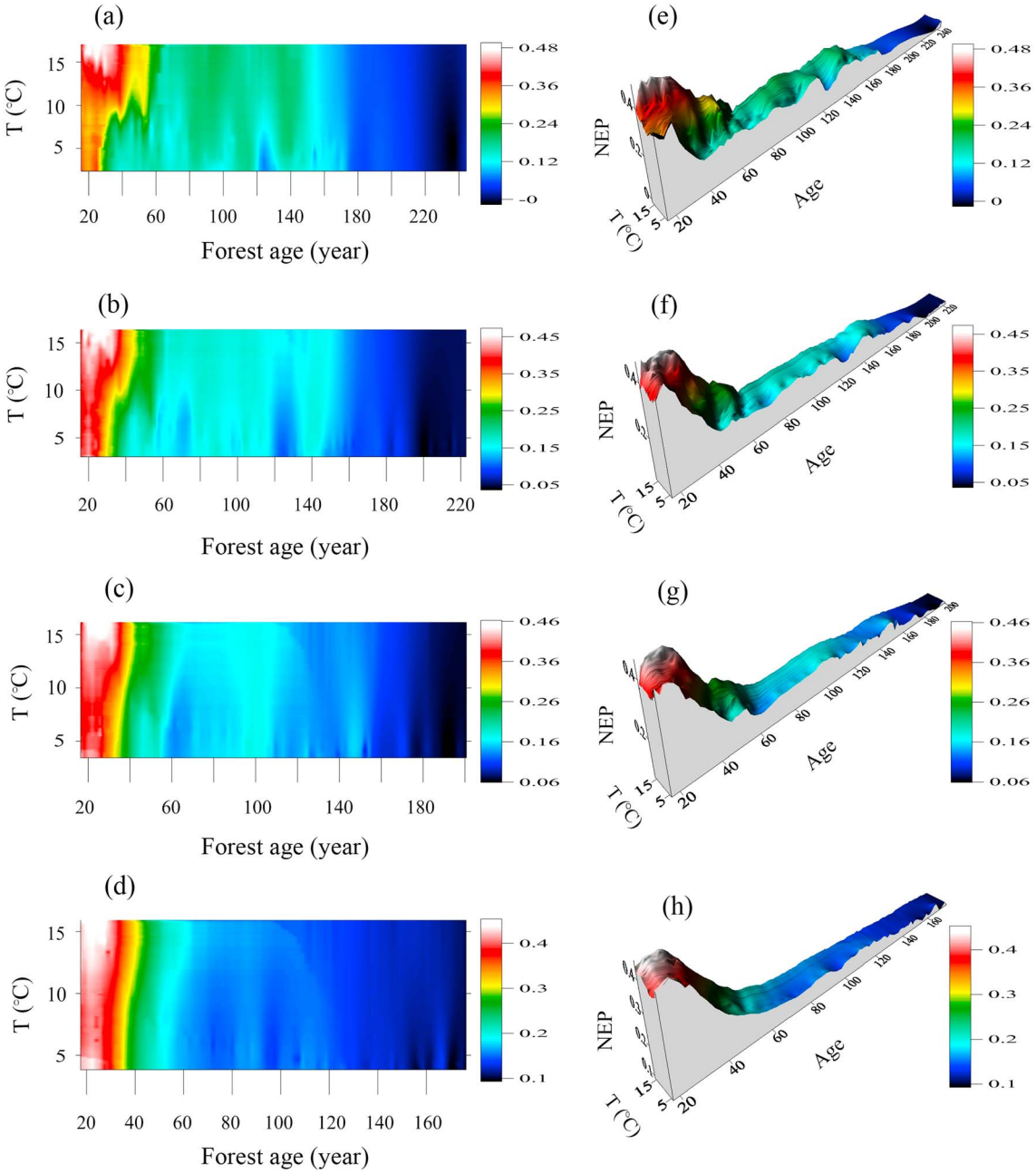

Figure 12. Illustration of different sizes of subsets on the apparent relationship between NEP and age. (a–d) Interactions of forest age and temperature on NEP and their change with subset sizes (i.e., *d* values) of 2.5, 5.0, 10, and 20% of total observations, respectively; (e–h) corresponding three-dimensional profiles, from which the long-term relationship between carbon sink and forest age could be illustrated. In general, forest age was the main factor controlling the long-term trend of the carbon sink.

(Rh)). Given the positive correlation between NPP and Rh, the ratio of NEP over NPP is commonly used to reflect the efficiency of a C sink per unit NPP [*Fang et al.*, 2007]. For evergreen needle-leaved forest in China, the C sink efficiency changes with forest age, first increasing and then decreasing (Figure 10). The highest efficiency is above 60%, occurring in young and half-mature forests with ages between 11 and 43 years. After that, the efficiency value decreases rapidly.

To evaluate the accumulated effect of multiyear C sink, we calculated the multiyear-averaged efficiency (i.e., the ratio of multiyear total C sink to multiyear total NPP), which is a reference index of optimal forest management (e.g., forest harvest time) from biological viewpoint [*Tietenberg*, 2005], and found that the

peak multiyear mean C sink efficiency appears at a forest age of 42 years, after which the yearly C sink efficiency is less than the multiyear-averaged values (i.e., 61.5%).

3.6. Sensitivity Analysis of Sample Size on Parameter Estimation

We conducted a sensitivity analysis to evaluate impacts of sample size (i.e., *d* value) on estimated age-dependent C sink. The sample size does not impact the relationship of C sink with forest age, although a large sample size tends to generate a smoother scatterplot than that with a small sample size (Figure 11). For instance, the variation of scatter points estimated by a sample size of 30% of total observations is much smaller than that for a 2.5% sample size. Nevertheless, the statistical curves inferred from the two sets of scatter points do not differ much (Figure 11). Thus, the estimated relationship between C sink and age is stable for different *d* values. A small sample with fewer sites tends to reflect more spatial heterogeneity of the local environment, increasing the variation of the estimated C sink. Large samples with more sites, however, tend to diminish these extrinsic environmental factors and make the estimated values closer to the expected value that controlled by the intrinsic age factor.

The potential impact of subset sizes on the NEP-age relationship (Figure 12) indicated that the interaction between forest age and temperature was related with the size of subset. In general, the long-term trend of the C sink was controlled by forest age and not impacted by the size of the subset (Figures 12e–12h). When forest age was the same, the temperature determined the NEP variations, especially for young and middle-aged forests. The interaction between forest age and temperature indicated that when the size of the subset increased, the impact of temperature on NEP decreased (Figures 12a–12d) and the intrinsic relationship (e.g., a suitable function) between NEP and age could be more easily revealed.

When the curve derived from a sample size of 20% is used as a reference, the root-mean-square error of the estimated C sink from sample sizes of 2.5%, 5%, 10%, and 30% is 0.006, 0.0084, 0.0055, and 0.0084 kg C m^{-2} yr^{-1}, respectively. Those amounts for only 3.2%, 4.5%, 2.9%, and 4.5% of the mean value of C sink (0.188 kg C m^{-2} yr^{-1}) for the ages from 0 to 160 years. Their variation ranges caused by sample sizes are comparable to the magnitude caused by climatic factors. A previous study found that climate explained approximately 5 ± 1% of the variability in C sink [*Luyssaert et al*., 2007].

4. Discussion

4.1. Age Dependence of Carbon Sink and NPP

NPP is one of the most important driving forces on C sequestration [*Zhou and Luo*, 2008; *He et al*., 2012; *Xia et al*., 2013]. Our results indicated that NPP and C sink are strongly correlated ($R^2 = 0.94$, $p < 0.001$) (Figure S4), which is consistent with the synthesized result from multisites conducted by *Pregitzer and Euskirchen* [2004] that revealed that the median NPP and C sink are strongly correlated ($R^2 = 0.83$, $p < 0.001$) across all biomes and age classes. A similar linear correlation has also been reported between the gross primary production and C sink across terrestrial vegetation types [*Law et al*., 2002; *Luyssaert et al*., 2007]. The correlation between gross ecosystem productivity (GEP) and NEP was also shown by flux tower observations. For example, observed NEP was significantly correlated with GEP, with 29% of the per-unit GEP contributed to NEP [*Yu et al*., 2013]. The high correlation between the modeled NPP and NEP is partly related to the model structure, where baseline C residence times are constants. Thus, the NPP-age relationship will propagate into the NEP-age relationship.

A suite of changes in structure and function is associated with age-related growth decline [*Tang et al*., 2014]. Foliage on older trees shows lower photosynthetic capacity and lower diurnal assimilation than foliage of younger trees [*Ryan et al*., 1997]. A synthesized result from multisites conducted by *Luyssaert et al*. [2008] indicated that both temperate and boreal forests show a pattern of declining NPP with forest age. Reduced leaf area and reduced photosynthetic capacity appear to be the most consistent features of this pattern, but the causes of these reductions in efficiency remain elusive and require direct examination and experimentation [*Ryan et al*., 1997; *Kashian et al*., 2013; *Stephenson et al*., 2014]. Research has indicated that the decline in pine NPP could be explained by reduced stomatal conductance and photosynthesis [*Drake et al*., 2011], which decreases the amount of C fixed per unit of light absorbed.

In this study, we applied a satellite-based light-use efficiency model, where the leaf area index was implicitly represented by the remote sensing-based NDVI, to optimize the photosynthetic capacity parameter (i.e., maximum light-use efficiency). Our results indicated that the decline in NPP was promoted by the decline

in growth efficiency (i.e., maximum light-use efficiency) and the decrease in NDVI. These results indicated that NPP is strongly correlated with the parameter of maximum light-use efficiency ($R^2 = 0.996$, $p < 0.001$) (Figure S4). The increase in NDVI also enhances the NPP with a high correlation ($R^2 = 0.93$, $p < 0.001$) (Figure S4).

4.2. Age Dependence of Vegetation and Soil Carbon Sink

Integrated analysis of the literature indicated that net ecosystem productivity (i.e., C sink) shows a rapid increase in young forests and then decreases gradually after reaching a peak [*Luyssaert et al*., 2008]. Biomass accumulation of vegetation pools declines after reaching a peak, but the degree and timing of the decline vary [*Ryan et al*., 1997]. Studies have indicated that the precise C dynamics vary by forest type, and the details remain poorly characterized [*Williams et al*., 2012]. In general, landscapes dominated by older stands are likely to be small C sinks with large C storage, even when current production declines [*Kasischke et al*., 1995; *Euskirchen et al*., 2002; *Pregitzer and Euskirchen*, 2004; *Luyssaert et al*., 2008].

Our results indicated that the forest age at the peak C sink (0.45 kg C m^{-2} yr^{-1}) is 22 years for evergreen needle-leaved forest in China, which is comparable with research conducted by *Thornton et al.* [2002], who reported that evergreen needle-leaved forests in the U.S. reach peak C sink values at ages of 8–19 years and only 2–7 years after becoming sinks. Similar results were found by *Coursolle et al*. [2012], indicating that the afforested white pine stands quickly became C sinks and offset initial C losses after 4 years and that the peak C sink for the afforested white pine was 0.69 kg C m^{-2} yr^{-1} at 15–20 years.

In this study, we found that the dynamic patterns of C sinks in vegetation and soil pools are significantly different at different stages. The vegetation C sink first increases with age and then decreases gradually. Soil C sink, however, increases continuously with forest age, with a role as a C source when the age is less than 20 years and a role of C sink after that.

The amount of the vegetation C sink and its change trend depends on the total C input (i.e., NPP) and the ratios of C allocation to slow turnover pools (i.e., stem), which have higher potential to sequester C in vegetation than other pools. Currently, C allocation is poorly understood, particularly in woody plants, where storage is large [*Cannell and Dewar*, 1994; *Zhou and Luo*, 2008]. The fraction of assimilated C available for wood production declined as woody biomass increased [*Ryan et al*., 1997]. Dense stands dominated by small trees yield more wood than stands dominated by fewer large trees, both because the relative growth rate of small trees is higher and because they are less likely to die [*Caspersen et al*., 2011].

Our study indicated that the high vegetation C sink for young forests and for half-mature forests is related to the higher maximum light-use efficiency, which decreases with age (Figure 6), and to the higher NPP allocation to wood, which also decreases with age (Figure 7). That is, the decreasing amount of ecosystem C input and the decreasing ratio of the wood pool, with a higher residence time, function together to decrease the magnitude of the vegetation C sink with age.

Although NPP and C sink in biomass decline rapidly with age, we found that the soil C sink persistently increases with age. Our results indicated that the soil of evergreen needle-leaved forest in China exhibits net soil C efflux when the forest age is less than 20 years, after which it becomes a C sink. This is comparable with the worldwide mean illustrated by the synthesized result from multisites, which indicated that the soil of young needle-leaved forests (age < 30 years) worldwide exhibits net C release [*Paul et al*., 2002; *Li et al*., 2012]. The rapid decrease of the ecosystem C sink after 20 years is related to the rapid decrease in input C (i.e., NPP). Soil C uptake has a lag effect, even when the vegetation C sink decreases, and the higher C input through litterfall and higher residence time in soil tends to produce a net C uptake. Because evergreen needle-leaved forest in China is a major forest type for the national afforestation projects and because most of these forests were planted in the past 10–30 years [*Zhou et al*., 2013], the long-term potential of the soil C sink is significant.

4.3. Efficiency of Ecosystem Carbon Sink and Its Implications for Forest Management

During the past few decades, the world's forests absorbed 2.4 Pg C yr^{-1} [*Pan et al*., 2011], and two thirds of these forests are managed [*Bellassen and Luyssaert*, 2014]. Because C sequestration in vegetation and soil pools show substantial differences in its magnitude, duration, and short- and long-term dynamics, the best way to manage forests to store C and to mitigate climate change has been hotly debated [*Bellassen and Luyssaert*, 2014]. Making good decisions about how to cultivate forests for climate change mitigation, such

as whether it is better to harvest or conserve trees, requires better understanding of the temporal patterns of forest C sinks in different pools.

Because increasing the size and age of trees and stands tends to reduce C assimilation [*Ryan et al*., 1997] and because forest wood can be a substitute for fossil fuels and carbon-intensive materials such as concrete and steel, one proposed forestry management strategy is to increase both forest stocks and timber harvest through measures such as protecting trees from herbivore consumption or replacing dying or low-productivity forests [*Bellassen and Luyssaert*, 2014]. In this study, we found that the temporal dynamics of vegetation C sink decrease greatly after approximately 50 years, and the harvest and reforestation would tend to increase C uptake efficiency and absorb more C from atmosphere if the harvested timber was used for long-lasting wood products. The highest C sink efficiency (i.e., the ratio of C sink to NPP) is approximately 60%, which appears in young and half-mature forests with ages between 11 and 43 years. In contrast, the maximum multiyear mean C sink efficiency appears at a forest age of 42 years, after which the yearly C sink efficiency drops below the multiyear-averaged values.

The timber harvest strategy, however, is most likely not feasible for soil C sequestration. The temporal dynamics of soil C sinks in this study indicated that soil acts as a C source when forest age is less than 20 years, after which it could constantly absorb C. The repeated deforestation and reforestation will negatively affect soil C uptake. Therefore, an optimal forest management for C sequestration must consider the dynamic patterns of both vegetation and soil pools, as well as the short-term and long-term efficiency of C uptake.

4.4. Sensitivities of Age-Dependent Carbon Residence Times on NEP Estimation

The parameters of residence times are quite crucial for modeling and predicting C dynamics [*Luo et al*., 2014; *Carvalhais et al*., 2014]. However, few studies revealed the quantitative relationship of C residence time and age at a large spatial scale; they usually estimate under steady state assumptions at regional [*Barrett*, 2002; *Zhou and Luo*, 2008] and global scales [*Chen et al*., 2013; *Carvalhais et al*., 2014]. Some studies found that C residence times for biomass pools were age dependent, as forest mortality increases with stand age [*Wirth et al*., 1999; *Xu et al*., 2012], but this relationship was found to saturate in very old forests [*Hudiburg et al*., 2009].

To reveal the potential impacts of age-dependent C residence times on estimations of C sink parameters and on the statistical model between NEP and forest age, we conducted a sensitivity analysis. We assumed that the parameters of C residence times for vegetation pools changed with age. That is, when forest age was >100 years, the parameters of C residence times for five biomass pools (i.e., stems, leaves, and three root pools) were constants; otherwise, their values increased linearly with decreasing age (i.e., young forest had relative higher residence times and lower mortality) at different rates (Formula 5):

$$\tau_{\text{age}} = \begin{cases} \tau_0 \cdot [1 + r \cdot (100 - \text{age})], & \text{age} < 100 \\ \tau_0, & \text{age} \geq 100 \end{cases}, \tag{5}$$

where τ_{age} is age-specific C residence times for vegetation pools; τ_0 is residence time for old forest that estimated from steady state assumption; and r is the rate of residence time change with age, respectively, equaling 0, 0.1, 0.2, 0.3, 0.4, and 0.5%. The age-specific residence times were used to estimated C sink parameters at step 3 and then compared with values estimated from the age-independent scheme.

The results indicated that when r increases from 0 to 0.5% (i.e., the possible maximum of τ increases from τ_0 to 1.5 τ_0), the magnitude of vegetation C sink increases, and accordingly, soil C sink decreases, especially for young forests (Figure S5). That is, the relatively higher C residence time for young forests tends to store more C in vegetation pools instead of soil pools. Revealing the age-dependent C residence times will help to evaluate the relative contribution of vegetation and soil C uptakes. Our sensitivity analysis also indicated that although age-dependent C residence time affected the proportion of vegetation and soil C sinks, it had little impact on the ecosystem total C sink (i.e., NEP) and the statistical relationship between NEP and age (Figure S5).

5. Conclusions

Forest ecosystem plays a significant role in C sequestration and its accumulation depends on forest age. Revealing the intrinsic relationship between forest age and C sink is crucial for reducing uncertainties of the predicted C sink potential. In this study, we developed a new stepwise data assimilation approach that synthesized process-based model, site-based biometric observation, and spatially explicit remote sensing

and GIS data sets and inversely estimated the quantitative relationship between forest C sink and forest age for evergreen needle-leaved forests in China. The study indicated that this stepwise data assimilation approach is effective on revealing quantitative relationship of age-dependence vegetation and soil C sinks. The results showed that ecosystem NEP increases rapidly with age and peaks at 0.451 kg C m^{-2} yr^{-1} at age 22, after which it gradually decreases. C sink in vegetation first increases rapidly with age and then decreases after peaking at 0.436 kg C m^{-2} yr^{-1}. C sink in soil, however, increases continuously with age. The forest age 20 is a turning point for soil, before which it is a C source and after which it is a C sink. The distinct difference between vegetation and soil C sinks implies that long-term forest management tends to increase soil carbon sink, unlike short-term afforestation and reforestation, which store C in vegetation pools. For the evergreen needle-leaved forest in China, the highest carbon sink efficiency (i.e., carbon sink per unit NPP) is approximately 60%, which appears in forests of ages between 11 and 43 years. This stepwise data assimilation method is worth extending to other regions to reveal the relationships between C sink and forest age from the biometric observations, especially where the chronosequence observations of C stocks and eddy flux observations are unavailable.

Acknowledgments

In line with the AGU publications data policy, the sources of site-related data can be accessed in section "2.1 Assimilated data" and GIS-related data can be accessed in section "2.2 Model drivers." The authors greatly appreciated constructive comments on the paper by Jianyang Xia, Junyi Liang, and Zheng Shi. This work was supported by the National Natural Science Foundation of China (41321001 and 41571185), the National Basic Research Program of China (2012CB955401), the New Century Excellent Talents in University (NCET-10-0251), and the Fundamental Research Funds for the Central Universities (2015KJJCB33). Y.L. was financially supported by U.S. Department of Energy, Terrestrial Ecosystem Sciences grant DE SC0008270 and U.S. National Science Foundation (NSF) grants DEB 0743778, DEB 0840964, EPS 0919466, and EF 1137293.

References

Acker, S., C. Halpern, M. Harmon, and C. Dyrness (2002), Trends in bole biomass accumulation, net primary production and tree mortality in *Pseudotsuga menziesii* forests of contrasting age, *Tree Physiol.*, *22*, 213–217.

Amiro, B. D., et al. (2010), Ecosystem carbon dioxide fluxes after disturbance in forests of North America, *J. Geophys. Res.*, *115*, G00K02, doi:10.1029/2010JG001390.

Anderson-Teixeira, K. J., A. D. Miller, J. E. Mohan, T. W. Hudiburg, B. D. Duval, and E. H. DeLucia (2013), Altered dynamics of forest recovery under a changing climate, *Global Change Biol.*, *19*, 2001–2021.

Baldocchi, D. (2008), Breathing of the terrestrial biosphere: Lessons learned from a global network of carbon dioxide flux measurement systems, *Aust. J. Bot.*, *56*, 1–26.

Baldocchi, D., et al. (2001), FLUXNET: A new tool to study the temporal and spatial variability of ecosystem-scale carbon dioxide, water vapor, and energy flux densities, *Bull. Am. Meteorol. Soc.*, *82*, 2415–2434.

Barford, C., S. C. Wofsy, M. L. Goulden, J. William Munger, E. Hammond Pyle, S. P. Urbanski, L. Hutyra, S. R. Saleska, D. Fitzjarrald, and K. Moore (2001), Factors controlling long- and short-term sequestration of atmospheric CO_2 in a mid-latitude forest, *Science*, *294*, 1688–1691.

Barrett, D. J. (2002), Steady state turnover time of carbon in the Australian terrestrial biosphere, *Global Biogeochem. Cycles*, *16*(4), 1108, doi:10.1029/2002GB001860.

Bellassen, V., and S. Luyssaert (2014), Managing forests in uncertain times, *Nature*, *506*, 153–155.

Bond-Lamberty, B., C. Wang, and S. T. Gower (2004), Net primary production and net ecosystem production of a boreal black spruce wildfire chronosequence, *Global Change Biol.*, *10*, 473–487.

Braswell, B. H., W. J. Sacks, E. Linder, and D. S. Schimel (2005), Estimating diurnal to annual ecosystem parameters by synthesis of a carbon flux model with eddy covariance net ecosystem exchange observations, *Global Change Biol.*, *11*, 335–355.

Cannell, M. G. R., and R. C. Dewar (1994), Carbon allocation in trees: A review of concepts for modeling, *Adv. Ecol. Res.*, *25*, 59–104.

Carvalhais, N., et al. (2008), Implications of the carbon cycle steady state assumption for biogeochemical modeling performance and inverse parameter retrieval, *Global Biogeochem. Cycles*, *22*, GB2007, doi:10.1029/2007GB003033.

Carvalhais, N., et al. (2014), Global covariation of carbon turnover times with climate in terrestrial ecosystems, *Nature*, *514*, doi:10.1038/nature13731.

Caspersen, J. P., M. C. Vanderwel, W. G. Cole, and D. W. Purves (2011), How stand productivity results from size- and competition-dependent growth and mortality, *PLoS One*, *6*, doi:10.1371/journal.pone.0028660.

Chapin, F. S., III, P. A. Matson, and H. A. Mooney (2002), *Principles of Terrestrial Ecosystem Ecology*, Springer, New York.

Chen, H. Y. H., and B. M. Shrestha (2012), Stand age, fire and clearcutting affect soil organic carbon and aggregation of mineral soils in boreal forests, *Soil Biol. Biochem.*, *50*, 149–157.

Chen, J. M., W. M. Ju, J. Cihlar, D. Price, J. Liu, W. Chen, J. Pan, A. Black, and A. Barr (2003), Spatial distribution of carbon sources and sinks in Canada's forests, *Tellus, Ser. B*, *55*, 622–641.

Chen, S., Y. Huang, J. Zou, and Y. Shi (2013), Mean residence time of global topsoil organic carbon depends on temperature, precipitation and soil nitrogen, *Global Planet. Change*, *100*, 99–108.

China Meteorological Administration (2015), China Meteorological Data Sharing Service System. [Available at http://cdc.nmic.cn/home.do, Accessed 6 June 2013.]

Coursolle, C., et al. (2012), Influence of stand age on the magnitude and seasonality of carbon fluxes in Canadian forests, *Agric. For. Meteorol.*, *165*, 136–148.

Covington, W. W. (1981), Changes in forest floor organic matter and nutrient content following clear cutting in northern hardwoods, *Ecology*, *62*, 41–48.

Drake, J. E., S. C. Davis, L. M. Raetz, and E. H. Delucia (2011), Mechanisms of age-related changes in forest production: The influence of physiological and successional changes, *Global Change Biol.*, *17*, 1522–1535.

Euskirchen, E. S., J. Chen, H. Li, E. J. Gustafson, and T. R. Crow (2002), Modeling landscape net ecosystem productivity (LandNEP) under alternative management regimes, *Ecol. Modell.*, *154*, 75–91.

Fang, J. Y., Z. D. Guo, S. L. Piao, and A. P. Chen (2007), Terrestrial vegetation carbon sinks in China, 1981–2000, *Sci. China Earth Sci.*, *50*, 1341–1350.

Field, C. B., J. T. Randerson, and C. M. Malmstrom (1995), Global net primary production: Combining ecology and remote sensing, *Remote Sens. Environ.*, *51*, 74–88.

Gough, C. M., C. S. Vogel, K. H. Harrold, K. George, and P. S. Curtis (2007), The legacy of harvest and fire on ecosystem carbon storage in a north temperate forest, *Global Change Biol.*, *13*, 1935–1949.

Goulden, M. L., A. M. S. Mcmillan, G. C. Winston, A. V. Rocha, K. L. Manies, J. W. Harden, and B. P. Bond-Lamberty (2011), Patterns of NPP, GPP, respiration, and NEP during boreal forest succession, *Global Change Biol.*, *17*, 855–871.

He, H., et al. (2014), Large-scale estimation and uncertainty analysis of gross primary production in Tibetan alpine grasslands, *J. Geophys. Res. Biogeosci.*, *119*, 466–486, doi:10.1002/2013JG002449.
He, L. M., J. M. Chen, Y. D. Pan, R. Birdsey, and J. Kattge (2012), Relationships between net primary productivity and forest stand age in U.S. forests, *Global Biogeochem. Cycles*, *26*, GB3009, doi:10.1029/2010GB003942.
Hember, R. A., W. A. Kurz, J. M. Metsaranta, T. A. Black, R. D. Guy, and N. C. Coops (2012), Accelerating regrowth of temperate-maritime forests due to environmental change, *Global Change Biol.*, *18*, 2026–2040.
Hudiburg, T., B. Law, D. Turner, J. Campbell, D. Donato, and M. Duane (2009), Carbon dynamics of Oregon and Northern California forests and potential land-based carbon storage, *Ecol. Appl.*, *19*, 163–180.
Hui, D., J. Wang, X. Le, W. Shen, and H. Ren (2012), Influences of biotic and abiotic factors on the relationship between tree productivity and biomass in China, *For. Ecol. Manage.*, *264*, 72–80.
Intergovernmental Panel on Climate Change (2007), *Climate Change 2007: The Physical Science Basis*, Cambridge Univ. Press, New York.
Jackson, R. B., J. Canadell, J. R. Ehleringer, H. A. Mooney, O. E. Sala, and E. D. Schulze (1996), A global analysis of root distributions for terrestrial biomes, *Oecologia*, *108*, 389–411.
Kashian, D. M., W. H. Romme, D. B. Tinker, M. G. Turner, and M. G. Ryan (2013), Postfire changes in forest carbon storage over a 300-year chronosequence of Pinus contorta-dominated forests, *Ecol. Monogr.*, *83*, 49–66.
Kasischke, E. S., N. L. Christensen, and B. J. Stocks (1995), Fire, global warming, and the carbon balance of boreal forests, *Ecol. Appl.*, *5*, 437–451.
Kuppel, S., P. Peylin, F. Chevallier, C. Bacour, F. Maignan, and A. D. Richardson (2012), Constraining a global ecosystem model with multi-site eddy-covariance data, *Biogeosciences*, *9*, 3757–3776.
Law, B. E., et al. (2002), Environmental controls over carbon dioxide and water vapor exchange of terrestrial vegetation, *Agric. For. Meteorol.*, *113*, 97–120.
Law, B. E., D. Turner, J. Campbell, O. J. Sun, S. V. Tuyl, W. D. Ritts, and W. B. Cohen (2004), Disturbance and climate effects on carbon stocks and fluxes across Western Oregon USA, *Global Change Biol.*, *10*, 1429–1444.
Law, B. E., D. Turner, M. Lefsky, J. Campbell, M. Guzy, O. Sun, S. V. Tuyl, and W. Cohen (2006), Carbon fluxes across regions: Observational constraints at multiple scales, in *Scaling and Uncertainty Analysis in Ecology: Methods and Applications*, edited by J. Wu et al., pp. 167–190, Springer, New York.
Li, D. J., S. Niu, and Y. Luo (2012), Global patterns of the dynamics of soil carbon and nitrogen stocks following afforestation: A meta-analysis, *New Phytol.*, *195*, 172–181.
Litton, C. M., J. W. Raich, and M. G. Ryan (2007), Carbon allocation in forest ecosystems, *Global Change Biol.*, *13*, 2089–2109.
Luo, T. X. (1996), Patterns of net primary productivity for Chinese major forest types and its mathematical models [in Chinese], PhD thesis, Institute of Geographic Sciences and Natural Resources Research, CAS, China.
Luo, Y., and E. Weng (2011), Dynamic disequilibrium of terrestrial carbon cycle under global change, *Trends Ecol. Evol.*, *26*, 96–104.
Luo, Y., L. W. White, J. G. Canadell, E. H. DeLucia, D. S. Ellsworth, A. Finzi, J. Lichter, and W. H. Schlesinger (2003), Sustainability of terrestrial carbon sequestration: A case study in Duke Forest with inversion approach, *Global Biogeochem. Cycles*, *17*(1), 1021, doi:10.1029/2002GB001923.
Luo, Y., K. Ogle, C. Tucker, S. Fei, C. Gao, S. LaDeau, J. S. Clark, and D. S. Schimel (2011), Ecological forecasting and data assimilation in a data-rich era, *Ecol. Appl.*, *21*, 1429–1442.
Luo, Y., T. F. Keenan, and M. Smith (2014), Predictability of the terrestrial carbon cycle, *Global Change Biol.*, doi:10.1111/gcb.12766.
Luyssaert, S., et al. (2007), CO2 balance of boreal, temperate, and tropical forests derived from a global database, *Global Change Biol.*, *13*, 2509–2537.
Luyssaert, S., E. -D. Schulze, A. Börner, A. Knohl, D. Hessenmöller, B. E. Law, P. Ciais, and J. Grace (2008), Old-growth forests as global carbon sinks, *Nature*, *455*, 213–215.
Pan, Y., et al. (2011), A large and persistent carbon sink in the world's forests, *Science*, *333*, 988–993.
Paul, K. I., P. J. Polglase, J. G. Nyakuengama, and P. K. Khanna (2002), Change in soil carbon following afforestation, *For. Ecol. Manage.*, *168*, 241–257.
Peichl, M., M. A. Arain, and J. J. Brodeur (2010), Age effects on carbon fluxes in temperate pine forests, *Agric. For. Meteorol.*, *150*, 1090–1101.
Potter, C. S., J. T. Randerson, C. B. Field, P. A. Matson, P. M. Vitousek, H. A. Mooney, and S. A. Klooster (1993), Terrestrial ecosystem production: A process model based on global satellite and surface data, *Global Biogeochem. Cycles*, *7*, 811–841, doi:10.1029/93GB02725.
Pregitzer, K. S., and E. S. Euskirchen (2004), Carbon cycling and storage in world forests: Biome patterns related to forest age, *Global Change Biol.*, *10*, 2052–2077.
Raupach, M. R., et al. (2005), Model-data synthesis in terrestrial carbon observation: Methods, data requirements and data uncertainty specification, *Global Change Biol.*, *2005*(11), 378–397.
Raymond, C. L., and D. McKenzie (2013), Temporal carbon dynamics of forests in Washington, U.S.: Implications for ecological theory and carbon management, *For. Ecol. Manage.*, *310*, 796–811.
Ryan, M. G., D. Binkley, and J. H. Fownes (1997), Age-related decline in forest productivity: Pattern and process, *Adv. Ecol. Res.*, *27*, 213–262.
Ryan, M. G., D. Binkley, J. H. Fownes, C. P. Giardina, and R. S. Senock (2004), An experimental test of the causes of forest growth decline with stand age, *Ecol. Monogr.*, *74*, 393–414.
Schaefer, K., et al. (2012), A model-data comparison of gross primary productivity: Results from the North American Carbon Program site synthesis, *J. Geophys. Res.*, *117*, G03010, doi:10.1029/2012JG001960.
Scharlemann, J. P. W., E. V. J. Tanner, R. Hiederer, and V. Kapos (2014), Global soil carbon: Understanding and managing the largest terrestrial carbon pool, *Carbon Manage.*, *5*, 81–91.
Shangguan, W., et al. (2013), A China data set of soil properties for land surface modeling, *J. Adv. Model. Earth Syst.*, *5*, 212–224, doi:10.1002/jame.20026.
Stephenson, N. L., et al. (2014), Rate of tree carbon accumulation increases continuously with tree size, *Nature*, doi:10.1038/nature12914.
Tang, J., S. Luyssaert, A. D. Richardson, W. Kutsch, and I. Janssens (2014), Steeper declines in forest photosynthesis than respiration explain age-driven decreases in forest growth, *Proc. Natl. Acad. Sci. U.S.A.*, doi:10.1073/pnas.1320761111.
Thornton, P. E., et al. (2002), Modeling and measuring the effects of disturbance history and climate on carbon and water budgets in evergreen needleleaf forests, *Agric. For. Meteorol.*, *113*, 185–222.
Tian, H., et al. (2015), Global patterns and controls of soil organic carbon dynamics as simulated by multiple terrestrial biosphere models: Current status and future directions, *Global Biogeochem. Cycles*, *29*, 775–792, doi:10.1002/2014GB005021.
Tietenberg, T. (2005), *Environmental and Natural Resource Economics*, 6th ed., Pearson Education Asia Limited and Tsinghua Univ. Press, Beijing.

Tucker, C. J., J. E. Pinzon, and M. E. Brown (2004), *Global Inventory Modeling and Mapping Studies*, *NA94apr15b.n11-Vlg, 2.0*, Global Land Cover Facility, Univ. of Maryland, College Park, Md.

Viscarra Rossel, R. A., R. Webster, E. N. Bui, and J. A. Baldock (2014), Baseline map of organic carbon in Australian soil to support national carbon accounting and monitoring under climate change, *Global Change Biol.*, *20*, 2953–2970.

Wang, S. Q., L. Zhou, J. Chen, W. Ju, X. Feng, and W. Wu (2011), Relationships between net primary productivity and stand age for several forest types and their influence on China's carbon balance, *J. Environ. Manage.*, *92*, 1651–1662.

Wang, Y. P., R. Leuning, H. A. Cleugh, and P. A. Coppin (2001), Parameter estimation in surface exchange models using non-linear inversion: How many parameters can we estimate and which measurements are most useful?, *Global Change Biol.*, *7*, 495–510.

Wang, Y. P., C. M. Trudinger, and I. G. Enting (2009), A review of applications of model-data fusion to studies of terrestrial carbon fluxes at different scales, *Agric. For. Meteorol.*, *149*, 1829–1842.

Williams, C. A., G. J. Collatz, J. Masek, and S. N. Goward (2012), Carbon consequences of forest disturbance and recovery across the conterminous United States, *Global Biogeochem. Cycles*, *26*, GB1005, doi:10.1029/2010GB003947.

Wirth, C. (2009), Old-growth forests: Function, fate and value, in *Old-Growth Forests*, *Ecol. Studies*, vol. 207, edited by C. Wirth, G. Gleixner, and M. Heimann, pp. 465–491, Springer, Berlin.

Wirth, C., et al. (1999), Above-ground biomass and structure of pristine Siberian Scots pine forests as controlled by competition and fire, *Oecologia*, *121*, 66–80.

Wutzler, T., and N. Carvalhais (2014), Balancing multiple constraints in model-data integration: Weights and the parameter block approach, *J. Geophys. Res. Biogeosci.*, *119*, 2112–2129, doi:10.1002/2014JG002650.

Xia, J., Y. Luo, Y. Wang, and O. Hararuk (2013), Traceable components of terrestrial carbon storage capacity in biogeochemical models, *Global Change Biol.*, *19*, 2104–2116.

Xu, C. Y., M. H. Turnbull, D. T. Tissue, J. D. Lewis, R. Carson, W. S. F. Schuster, D. Whitehead, A. S. Walcroft, J. Li, and K. L. Griffin (2012), Age-related decline of stand biomass accumulation is primarily due to mortality and not to reduction in NPP associated with individual tree physiology, tree growth or stand structure in a Quercus-dominated forest, *J. Ecol.*, *100*, 428–440, doi:10.1111/j.1365-2745.2011.01933.x.

Xu, T., L. White, D. Hui, and Y. Luo (2006), Probabilistic inversion of a terrestrial ecosystem model: Analysis of uncertainty in parameter estimation and model prediction, *Global Biogeochem. Cycles*, *20*, GB2007, doi:10.1029/2005GB002468.

Yang, Y. H., Y. Luo, and A. C. Finzi (2011), Carbon and nitrogen dynamics during forest stand development: A global synthesis, *New Phytol.*, *190*, 977–989.

Yu, G. R., et al. (2013), Spatial patterns and climate drivers of carbon fluxes in terrestrial ecosystems of China, *Global Change Biol.*, *19*, 798–810.

Yu, G., Z. Chen, S. Piao, C. Peng, P. Ciais, Q. Wang, X. Li, and X. Zhu (2014), High carbon dioxide uptake by subtropical forest ecosystems in the East Asian monsoon region, *Proc. Natl. Acad. Sci. U.S.A.*, doi:10.1073/pnas.1317065111.

Yuan, W., S. Liang, S. Liu, E. Weng, Y. Luo, D. Hollinger, and H. Zhang (2012), Improving model parameter estimation using coupling relationships between vegetation production and ecosystem respiration, *Ecol. Model.*, *240*, 29–40.

Zhou, T., and Y. Luo (2008), Spatial patterns of ecosystem carbon residence time and NPP-driven carbon uptake in the conterminous United States, *Global Biogeochem. Cycles*, *22*, GB3032, doi:10.1029/2007GB002939.

Zhou, T., P. Shi, G. Jia, X. Li, and Y. Luo (2010), Spatial patterns of ecosystem carbon residence time in Chinese forests, *Sci. China Earth Sci.*, *53*, 1229–1240.

Zhou, T., P. Shi, G. Jia, and Y. Luo (2013), Nonsteady state carbon sequestration in forest ecosystems of China estimated by data assimilation, *J. Geophys. Res. Biogeosci.*, *118*, 1369–1384, doi:10.1002/jgrg.20114.

Zhu, W. Q., Y. Z. Pan, H. He, Y. Deyong, and H. Haibo (2006), Simulation of maximum light use efficiency for some typical vegetation types in China, *Chin. Sci. Bull.*, *51*, 457–463.